10th World Congress on Structural and Multidisciplinary Optimization
May 19 -24, 2013, Orlando, Florida, USA

Optimal topology design of continuum structures with stress concentration alleviation via level set method

Weisheng Zhang[1], Xu Guo[1] , Michael Yu Wang[2]

[1] State Key Laboratory of Structural Analysis for Industrial Equipment Department of Engineering Mechanics
Dalian University of Technology, Dalian, P.R. China, dr.vincent.zhang@gmail.com
[2] Department of Mechanical and Automation Engineering The Chinese University of Hong Kong Shatin, NT, Hong Kong

1. Abstract
Although the phenomenon of stress concentration is of paramount importance to engineers when they are designing load-carrying structures, stiffness is often used as the solely concerned objective or constraint function in the studies of optimal topology design of continuum structures. Sometimes this will lead to optimal designs with severe stress concentrations which may be highly responsible for the fracture, creep and fatigue of structures. Thus, considering stress-related objective or constraint functions in topology optimization problems is very important from both theoretical and application perspectives. It has been known, however, that this kind of problem is very challenging since several difficulties must be overcome in order to solve it effectively. The first difficulty stems from the fact that stress constrained topology optimization problems always suffer from the so-called singularity problem. The second difficulty in stress-related optimization problem is due to the high computational cost caused by the large number of local stress constraints. The conventional treatment of this difficulty with use of the so-called global stress measures cannot give an adequate control of the magnitude of local stress level. The third difficulty is related to the accuracy of stress computation which is greatly influenced by the local geometry of structure.
The aim of the present work is to develop some effective numerical techniques for designing stiff structures with less stress concentrations. This is achieved by introducing some specific stress measures, which are sensitive to the existence of high local stresses, in the problem formulation and resolving the corresponding optimization problem numerically in a level set framework. In the first global stress measure, local geometry information such as boundary curvature is introduced while in the second global stress measure, stress gradient is employed to locate the hot points of high local stresses automatically. Our study indicates that with use of the proposed numerical schemes and proposed global stress measures, the intrinsic difficulties mentioned above in stress-related topology optimization of continuum structures can be overcome in a natural way.
2. Keywords: Topology Optimization; Stress concentration; Level set; Extended finite element method (X-FEM)

3. Introduction
The study of topology optimization has received tremendous attention since the pioneering work of Bendsoe and Kikuchi [1]. Topology optimization aims at optimizing the material layout of a structure within a given design space under prescribed load and boundary conditions such that some design criteria are satisfied. Nowadays, numerous methods have been proposed for optimal topology design and topology optimization has been recognized as a very powerful tool to help engineers obtain innovative conceptual designs that cannot be created easily through size and shape optimizations. A state of the art review and some recent developments in this rapidly developing field can be found in the review articles [2-4] and the references therein.
Although remarkable achievements have been made in the field of topology optimization, it is worth noting that most of the studies have been devoted to the compliance minimization problems. In practical engineering applications, however, the consideration of stress criteria is indispensible and should be dealt with seriously. Theoretical analyses [5] also indicated that the optimal designs obtained under maximum stiffness and maximum strength considerations, respectively, may be quite different. Furthermore, as pointed out in [6], compared with compliance minimization problems, the solution of stress-related topology optimization problems is much more challenging. The complexity comes from both the theoretical and numerical solution aspects. One difficulty is associated with the so-called singularity phenomenon resulting from the discontinuity of local stress constraints [7]. Many studies showed that singularity phenomenon may prevent numerical optimization algorithms (especially those using gradient information) from finding the true optimal topology if it cannot be handled in a mathematical appropriate way. Another difficulty is related to the computational efforts involved in the solution of stress-related topology optimization problems. When local stress measures are considered, it is required that the magnitude of the stress measure should not exceed a prescribed upper bound at every material point in the structure. Under this circumstance, it is often impossible to deal with the stress constraints point wisely at every

step of numerical optimization and an active–set strategy is often employed to save the computational cost. But this will sometimes lead to the oscillation or even divergence of a solution process. Another technique often used to reduce the computational cost is to introduce some global stress measures (often in the form of integral) into the problem formulation intending to restrain the magnitude of local stress implicitly. Although this approach is very effective to reduce the overall stress level, it is difficult to give a precise control of the maximum stress in the structure. Driven by the impetus to resolve this both practically important and academically challenging problem, an ever-increasing research attention has been paid to the stress-related topology optimization in recent years.

Recent years have also witnessed a growing interest of solving stress-related topology optimization problems with level set-based method. Allaire and Jouve [8] considered the problem of minimum stress topology design using level set approach. In their work, global stress measure in integral form was adopted as the objective function. Guo et al. [9] demonstrated that level set-based approach is a promising tool for the solution of stress-related optimal topology design under appropriate problem formulations. They also pointed out that global structural performance measure should be included into the problem formulation when local stress constraints are considered in order to regularize the solution process.

The present paper is devoted to developing some effective numerical techniques for designing stiff structures with less stress concentrations in a computational efficient way. This is achieved by introducing a new global stress measures into the problem formulation with which the local stress level can be controlled effectively. The adoption of level set-based approach stems from our previous experience such that it has some natural advantages when applied to stress related topology optimization problems.

4. Problem statement and the new global stress measures

4.1. Problem statement and its mathematical formulation

In this study, we will consider optimal topology design of continuum structures with less stress concentrations using global stress measures in the level set framework. In such a case, the optimization problem can be formulated mathematically as follows:

$$\begin{aligned}
&\text{Find } \phi(\boldsymbol{x}) \in \mathrm{L}^{\infty}(\mathrm{D}), \boldsymbol{u}(\boldsymbol{x}) \in \mathbf{H}^{1}(\mathrm{D}) \\
&\text{Min } \quad F\left(\phi(\boldsymbol{x}), \boldsymbol{\sigma}\left(\boldsymbol{\epsilon}(\boldsymbol{u}(\boldsymbol{x}))\right)\right) \\
&\text{s. t.} \\
&\int_{\mathrm{D}} \mathrm{H}(\phi(\boldsymbol{x}))\mathbb{E}:\boldsymbol{\epsilon}(\boldsymbol{u}):\boldsymbol{\epsilon}(\boldsymbol{v})\mathrm{dV} = \int_{\mathrm{D}} \mathrm{H}\big(\phi(\boldsymbol{x})\big)\boldsymbol{f}\cdot\boldsymbol{v}\mathrm{dV} + \int_{\Gamma_{\mathrm{t}}} \boldsymbol{t}\cdot\boldsymbol{v}\mathrm{dS}, \forall \boldsymbol{v} \in \mathrm{U}_{\mathrm{ad}}, \\
&\mathrm{V_s} - \overline{\mathrm{V}} = \int_{\mathrm{D}} \mathrm{H}\big(\phi(\boldsymbol{x})\big)\mathrm{dV} - \overline{\mathrm{V}} \le 0, \\
&\boldsymbol{u} = \overline{\boldsymbol{u}}, \quad \text{on } \Gamma_{\mathrm{u}}.
\end{aligned} \tag{4.1}$$

In Eq. (4.1), D is a prescribed design domain in which the optimal material distribution is seeking for.$\mathrm{H}(x)$ is the Heaviside function: $\mathrm{H}(x) = 1,\ if\ x \ge 0\ and\ \mathrm{H}(x) = 0, otherwise$. $\phi(\boldsymbol{x})$ is the level set function characterizing the material distribution in D and $\boldsymbol{u}(\boldsymbol{x})$ is the displacement field of the corresponding boundary value problem defined on $\Omega_{\mathrm{s}} = \{\boldsymbol{x} \in \mathrm{D} | \phi(\boldsymbol{x}) \ge 0\}$, respectively. $\boldsymbol{v}(\boldsymbol{x})$ represents the test function and $\mathrm{U_{ad}} = \{\boldsymbol{v}(\boldsymbol{x}) | \boldsymbol{v}(\boldsymbol{x}) \in \mathbf{H}^{1}(\mathrm{D}),\ \boldsymbol{v}(\boldsymbol{x}) = \boldsymbol{0} \text{ on } \Gamma_{\mathrm{u}}\}$ is the admissible set $\boldsymbol{v}$ belongs to. $\boldsymbol{f}$ and $\boldsymbol{t}$ denote the body force density and the traction force on Neumann boundary Γ_{t}, respectively. $\overline{\boldsymbol{u}}$ is the prescribed displacement on Dirichlet boundary Γ_{u}. $\mathbb{E} = (E_{ijkl}) = E^{s}/(1+\nu^{s})[\mathbb{I} + \nu^{s}/(1-2\nu^{s})\boldsymbol{\delta}\otimes\boldsymbol{\delta}]$ ($\mathbb{I}$ and $\boldsymbol{\delta}$ denote the fourth and second order identity tensor, respectively) is the fourth order isotropic elasticity tensor of the given solid material. E^{s} and ν^{s} are the corresponding Young's modulus and Poisson's ratio, respectively. $\boldsymbol{\epsilon}(\boldsymbol{u}) = \mathrm{sym}(\nabla\boldsymbol{u})$ is the linear strain tensor. $F\left(\phi(\boldsymbol{x}), \boldsymbol{\sigma}\left(\boldsymbol{\epsilon}(\boldsymbol{u})\right)\right)$ is a global stress measure, which is a functional of ϕ and $\boldsymbol{\sigma}$. $\overline{\mathrm{V}}$ denotes the prescribed upper bound on $\mathrm{V_s}$, which represents the total volume of the solid material. Moreover, in order to simplify the analysis, in the present study, Γ_{u} and the part of Neumann boundary Γ_{t} where $\boldsymbol{t} \neq \boldsymbol{0}$ are assumed to be non-designable. Without loss of generality, only 2D case is considered.

4.2. Global stress measure enhanced by stress gradient information

In fact the discontinuities of the distribution of applied forces, the boundary conditions and the material properties can all serve as the sources of stress concentrations. In view of this, the following global stress measure

$$F^{*}(\phi(\boldsymbol{x}), \boldsymbol{\sigma}) = \int_{\mathrm{D}} \mathrm{H}(\phi) G(\nabla\boldsymbol{\sigma}) \mathcal{H}(\sigma_{\mathrm{M}} - \overline{\sigma})\mathrm{dV} \tag{4.2}$$

is suggested to restrain the local stress level below a prescribed upper bound $\overline{\sigma}$. In Eq. (4.2), $G(\nabla\boldsymbol{\sigma})$ is a function of the gradient of the stress tensor and the function $\mathcal{H}(x)$ is defined as

$$\mathcal{H}(x) = \begin{cases} x^2, & x \geq 0, \\ 0\ , & x < 0. \end{cases} \tag{4.3}$$

It can be verified that $\mathcal{H}(x)$ is differentiable on $(-\infty, +\infty)$. From Eq. (4.2), it can be observed that F^* will be equal to zero if $\sigma_{\mathrm{M}} \leq \overline{\sigma}$ almost everywhere in the structure. Furthermore, theoretical analysis and numerical experiments indicate that stress gradient is always very large in the region where severe stress concentration exists. Therefore the weight function $G(\nabla\boldsymbol{\sigma})$ with an appropriate form of in Eq. (4.2) can serve as both the indicator and the magnification factor of stress concentrations. We take $G(\nabla\boldsymbol{\sigma})$ in the following form:

$$G(\nabla\boldsymbol{\sigma}) = \|\nabla\sigma_{xx}\|^2 + \left\|\nabla\sigma_{yy}\right\|^2 + \left\|\nabla\sigma_{xy}\right\|^2. \tag{4.4}$$

When F^* is used as the global stress measure, we propose to formulate the corresponding local stress-constrained topology optimization as follows:

$$\begin{gathered} \text{Find } \phi(\boldsymbol{x}) \in \mathrm{L}^{\infty}(\mathrm{D}), \boldsymbol{u}(\boldsymbol{x}) \in \mathbf{H}^1(\mathrm{D}) \\ \text{Min} \qquad c = \int_{\mathrm{D}} \mathrm{H}(\phi(\boldsymbol{x}))\mathbb{E}\colon\boldsymbol{\epsilon}(\boldsymbol{u})\colon\boldsymbol{\epsilon}(\boldsymbol{u})\mathrm{dV} \\ \text{s. t.} \\ \int_{\mathrm{D}} \mathrm{H}(\phi(\boldsymbol{x}))\mathbb{E}\colon\boldsymbol{\epsilon}(\boldsymbol{u})\colon\boldsymbol{\epsilon}(\boldsymbol{v})\mathrm{dV} = \int_{\mathrm{D}} \mathrm{H}\big(\phi(\boldsymbol{x})\big)\boldsymbol{f}\cdot\boldsymbol{v}\mathrm{dV} + \int_{\Gamma_{\mathrm{t}}} \boldsymbol{t}\cdot\boldsymbol{v}\mathrm{dS}, \forall\boldsymbol{v} \in \mathrm{U}_{\mathrm{ad}}, \\ \mathrm{V_s} - \overline{\mathrm{V}} = \int_{\mathrm{D}} \mathrm{H}\big(\phi(\boldsymbol{x})\big)\mathrm{dV} - \overline{\mathrm{V}} \leq 0, \\ F^*\left(\phi(\boldsymbol{x}), \boldsymbol{\sigma}\big(\boldsymbol{\epsilon}(\boldsymbol{u}(\boldsymbol{x}))\big)\right) = \int_{\mathrm{D}} \mathrm{H}(\phi) f(\nabla\boldsymbol{\sigma})\mathcal{H}(\sigma_{\mathrm{M}} - \overline{\sigma})\mathrm{dV} \leq 0, \\ \boldsymbol{u} = \overline{\boldsymbol{u}}, \quad \text{on } \Gamma_{\mathrm{u}}. \end{gathered} \tag{4.5}$$

In Eq. (4.5), the compliance of the structures is used as the objective functional. As pointed out in [9], this can help to regularize the optimization process carried out in level set framework. $F^* \leq 0$ in Eq. (4.5) is used to impose the point-wise local stress constraint $\sigma_{\mathrm{M}} \leq \overline{\sigma}$ implicitly. It is also worth noting that the form of $\mathcal{H}(x)$ is not unique. Other forms such as

$$\mathcal{H}_q(x) = \begin{cases} x^q, & x \geq 0, \\ 0\ , & x < 0 \end{cases}$$

with $q > 0$ can also be used to serve the purpose of local stress control. Numerical experiments support this argument.

5. Numerical solution aspects

5.1. Shape sensitivity analysis

In level set-based topology optimization approach, shape derivative is required for numerical implementation. By introducing a virtual time parameter t, the time dependent level set function ϕ can be written as $\phi = \phi(\boldsymbol{x}, t)$. Under this circumstance, both the objective and constraint functional can be viewed as functions of t, that is

$$\mathcal{F}(t) = F\big(\phi(\boldsymbol{x}, t), \boldsymbol{\sigma}^{\phi}(\boldsymbol{x}, t)\big) = F\left(\phi(\boldsymbol{x}, t), \boldsymbol{\sigma}\left(\boldsymbol{\epsilon}\big(\boldsymbol{u}^{\phi}(\boldsymbol{x}, t)\big)\right)\right), \tag{5.1}$$

where $\boldsymbol{u}^{\phi} = \boldsymbol{u}^{\phi}(\boldsymbol{x}, t)$ is the displacement field of the corresponding boundary value problem defined on $\Omega_{\mathrm{s}}(\boldsymbol{x}, t) = \{\boldsymbol{x} \in \mathrm{D} | \phi(\boldsymbol{x}, t) 0\}$. The shape derivative is therefore can be viewed as the total time derivative of $\mathcal{F}(t)$, i.e., $\mathrm{d}\mathcal{F}(t)/\mathrm{d}t$. In the following discussions, for the sake of simplicity, it is assumed in the following that $\mathbb{E}$ and t are spatial invariant (i.e., their spatial derivative $(\mathbb{E})'$ and $(\boldsymbol{t})'$ are equal to zero), body force is neglected (i.e., $\boldsymbol{f} = \boldsymbol{0}$), $\overline{\boldsymbol{u}} = \boldsymbol{0}$, $\Gamma_{\mathrm{u}} \cap \Gamma_{\mathrm{v}} = \emptyset$ and $\Gamma_{\mathrm{t}}(\text{where } \boldsymbol{t} \neq \boldsymbol{0}) \cap \Gamma_{\mathrm{v}} = \emptyset$. Here Γ_{v} denotes the designable part of the structural boundary.

As regard to the stress measure F^*, the corresponding shape derivative can be calculated as

$$\frac{\mathrm{d}\mathcal{F}^*(t)}{\mathrm{d}t} = \int_{\Gamma_{\mathrm{v}} \cap \mathrm{S}} \left(-\mathbb{E}\colon\nabla\boldsymbol{u}^{\phi}\colon\nabla\boldsymbol{w}^{\phi} + G\big(\widetilde{\nabla\boldsymbol{\sigma}}\big)\mathcal{H}(\sigma_{\mathrm{M}} - \overline{\sigma})\big|_{\boldsymbol{u}=\boldsymbol{u}^{\phi}}\right)(\boldsymbol{V}\cdot\boldsymbol{n})\mathrm{dS}, \tag{5.2}$$

where $\boldsymbol{w}^{\phi}$ is the solution of the following adjoint boundary value problem defined on $\Omega_{\mathrm{s}}(\boldsymbol{x}, t) = \{\boldsymbol{x} \in \mathrm{D} | \phi(\boldsymbol{x}, t) \geq 0\}$:

$$\begin{gathered} \text{Find} \quad \boldsymbol{w}^{\phi} \in \mathbf{H}^1(\mathrm{D}) \\ \text{such that} \\ \int_{\mathrm{D}} \mathrm{H}(\phi)\mathbb{E}\colon\nabla\boldsymbol{w}^{\phi}\colon\nabla\boldsymbol{v}\mathrm{dV} = \int_{\mathrm{D}} \mathrm{H}(\phi) \left.\frac{\partial\left(G\big(\widetilde{\nabla\boldsymbol{\sigma}}\big)\mathcal{H}(\sigma_{\mathrm{M}} - \overline{\sigma})\right)}{\partial\boldsymbol{\sigma}}\right|_{\boldsymbol{u}=\boldsymbol{u}^{\phi}} \colon\mathbb{E}\colon\boldsymbol{\epsilon}(\boldsymbol{v})dV + \end{gathered}$$

$$\int_{\mathrm{D}} \mathrm{H}(\phi) \left. \frac{\partial \left(G(\widetilde{\nabla \boldsymbol{\sigma}}) \mathcal{H}(\sigma_{\mathrm{M}} - \overline{\sigma}) \right)}{\partial \widetilde{\nabla \boldsymbol{\sigma}}} \right|_{\boldsymbol{u}=\boldsymbol{u}^{\phi}} \vdots \nabla(\widetilde{\mathbb{E}:\boldsymbol{\epsilon}(\boldsymbol{v})}) dV, \qquad \forall \boldsymbol{v} \in \mathrm{U}_{\mathrm{ad}},$$

$$\boldsymbol{w}^{\phi} = \mathbf{0}, \quad \text{on } \Gamma_{\mathrm{u}}. \tag{5.3}$$

In our numerical implementations, $\nabla(\mathbb{E}:\boldsymbol{\epsilon}(\boldsymbol{v}))$ has been used to replace $\nabla(\widetilde{\mathbb{E}:\boldsymbol{\epsilon}(\boldsymbol{v})})$ in Eq. (5.3) for the sake of simplicity. Note that since $\widetilde{\nabla \boldsymbol{\sigma}} \in \mathbf{C}(\bar{\Omega}_{\mathrm{s}})$, the second integration in the right hand of the virtual work equation in Eq. (5.3) is bounded even though $\nabla\left(\mathbb{E}:\left(\boldsymbol{\epsilon}(\boldsymbol{v})\right)\right) \in \mathbf{H}^{-1}(\mathrm{D})$.

Finally, the shape derivative of the structural compliance and volume can be calculated simply as:

$$\frac{\mathrm{dc}}{\mathrm{d}t} = \int_{\Gamma_{\mathrm{v}} \cap \mathrm{S}} \left(-\mathbb{E}:\nabla \boldsymbol{u}^{\phi}:\nabla \boldsymbol{u}^{\phi}\right)(\boldsymbol{V} \cdot \boldsymbol{n}) \mathrm{dS} \tag{5.4}$$

and

$$\frac{\mathrm{dV_s}}{\mathrm{d}t} = \frac{\mathrm{d}}{\mathrm{d}t} \int_{\mathrm{D}} \mathrm{H}(\phi) \mathrm{dV} = \int_{\Gamma_{\mathrm{v}} \cap \mathrm{S}} (\boldsymbol{V} \cdot \boldsymbol{n}) \mathrm{dS}, \tag{5.5}$$

respectively.

5.2. Finite element analysis

For stress-related topology optimization problems, it is of great importance to guarantee the accuracy of stress computation otherwise the reliability of the optimization results may be questionable. In the present study, the X-FEM approach proposed in [10] is adopted for the solution of the approximate primary and adjoint displacement fields (i.e., $\boldsymbol{u}$ and $\boldsymbol{w}$, respectively) with high accuracy without remeshing on the whole structure. For more details about the corresponding numerical implementations, we refer the readers to [10] and the references therein. As mentioned in the previous section, the right hand pseudo load vector for numerical solution of $\boldsymbol{w}^{\phi}$ is calculated element-wisely based on the right hand term in the virtual work expression.

6. Numerical examples

In this section, several numerical examples are presented to illustrate the effectiveness of the proposed global stress measures to obtain optimal topology designs with less stress concentrations. For illustration purpose, only 2D numerical examples under plane stress condition (with unit thickness) are considered in the present work. In all examples, the material, load and geometry data are chosen as dimensionless since the main purpose of the present study is to test the numerical performance of the proposed algorithm. The Young's modulus and the Poisson's ratio for solid material and weak material (mimicking void) are chosen as $E^s = 1$, $\nu^s = 0.3$ and $E^w = 1 \times 10^{-6}$, $\nu^w = 0.3$, respectively. Four-node bilinear square elements are adopted for finite element discretization of the primary and adjoint displacement fields. As usual, the same mesh is also used for the evolution of the level set function. Another issue worth mentioning is that the high local stresses induced by the concentrated external load and clamped boundary supports are not considered in the following examples since they cannot be reduced effectively through shape or topology optimizations. This is achieved by excluding the volume integration in F^* on small regions surrounding the above mentioned sources of stress singularity. Not that the stress distributions in these regions are also not shown in the stress contour plots. In all examples, the optimization process will terminate once no further improvement of the objective functional can be achieved (the relative fluctuation of the objective functional is less than 0.01 in 20 steps) and all constraints are satisfied (the relative violation is less than 0.001 in 20 steps).

6.1. A L-shaped beam problem

In this example, the classical L-shaped beam problem shown in Fig. 1 is examined to investigate the capability of the proposed global stress measures for local stress level control and stress concentration alleviation. For comparison purpose, first the classical compliance minimization problem is solved with $\overline{\mathrm{V}} = 0.2$ from the initial design shown in Fig. 2. The optimal structural topology and the corresponding stress distribution are shown in Fig. 3. From this figure, it is observed that the optimal compliance design has an almost 270^0 re-entrant corner. This is quite reasonable from stiffness maximization point of review since the cross sectional moment of inertia of the horizontal beam at the inner corner is large for this kind of configuration. However, this design is by no means optimal when stress-related performance measures are considered. It is found that there exists severe stress concentration at the re-entrant corner and the maximum von Mises stress is about 136.

Next, the same optimization problem is solved with use of the problem formulation in Eq. (4.5), where F^* is adopted as the constraint functional. This time it is intend to restrain the peak stress in the structure to be less than 70 (i.e., $\overline{\sigma} = 70$). Fig.4 plot the corresponding optimal designs and the stress distributions. The optimization results reveal that the peak stress in the structure can be controlled successfully with use of Eq. (4.5). The local stresses in the corresponding optimal structures are all below the prescribed upper bound.

Compared with compliance-based design, the maximum local stress in structure has been reduced by almost 50% in the stress-based design. It is also worth noting that in the classical treatments of local stress control through global stress measures, the introduction of some empirical or control parameters are always unavoidable. In some other treatments, penalty coefficients have also been used to exaggerate the violation of local stress constraints. It should be noticed that sometimes the choice of these parameters is highly problem-dependent and can only be determined through numerical experiments. On the other hand, there is no need to introduce any empirical or control parameters in our treatment of local stress constraints using the problem formulation presented in Eq. (4.5). Moreover, the introduction of $G(\nabla\boldsymbol{\sigma})$ in F^* can not only help to identify the region with severe stress concentration, but also facilitate distributing the stress uniformly. Typically, optimal designs with substantial local stress reduction can be obtained within 200 iteration steps. The detailed optimization results of this problem are reported in Table.1.

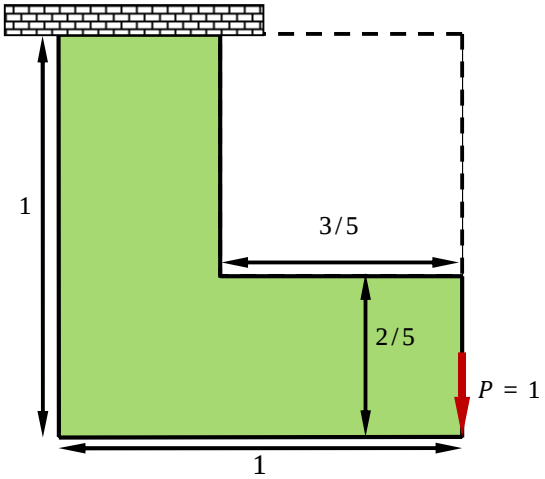

Fig. 1 Design domain of the L-shaped beam problem.

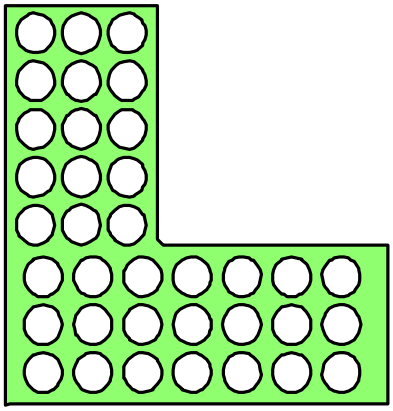
Fig. 2 Initial design of the L-shaped beam problem.

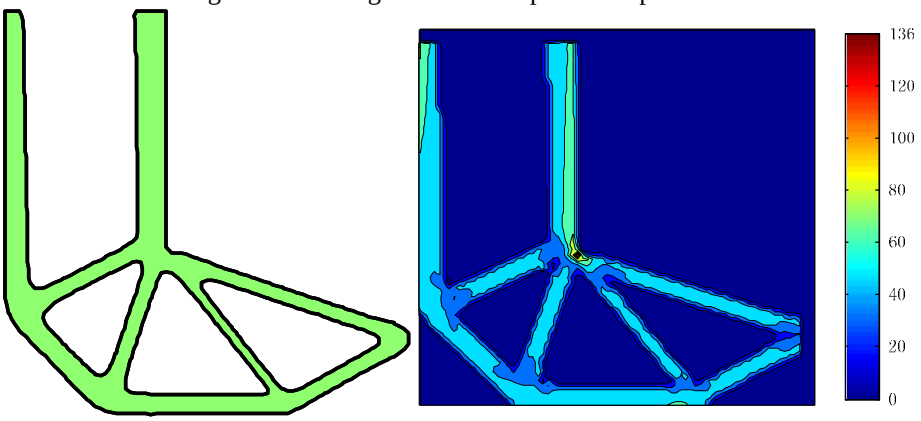

Fig. 3 Compliance-based optimal design of the L-shape beam problem and the corresponding stress distribution.

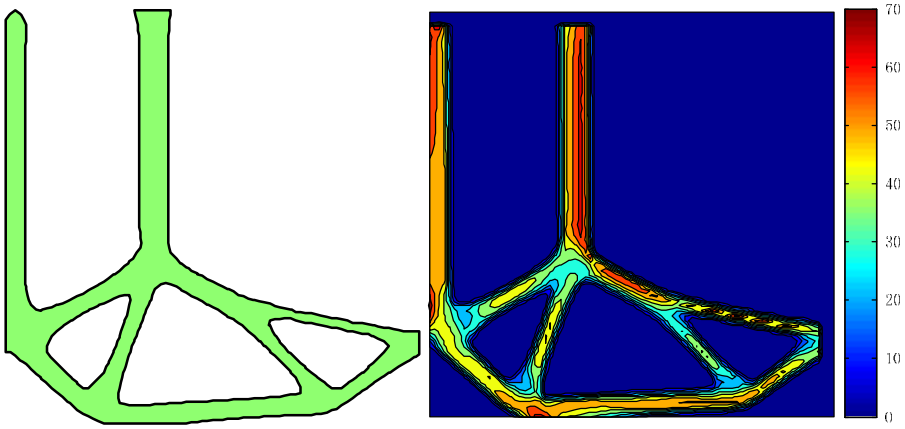

Fig. 4 Optimal design of the L-shape beam problem and the corresponding stress distribution with 80×80 mesh ($\overline{\sigma} = 70$) under formulation Eq. (4.5).

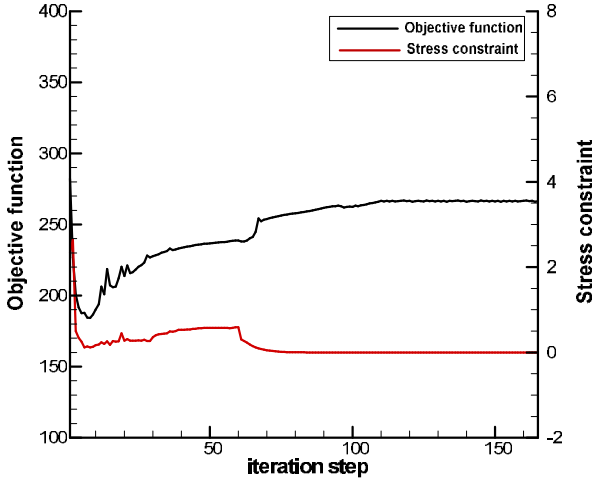

Fig. 5 Iteration history (80×80 mesh, $\overline{\sigma} = 70$).

Table.1 Optimization results for the L-shaped beam problem

	Compliance	Stress constraint	Maximum von Mises stress
Compliance minimization 80×80	243.73	/	136.14
80×80 with $\sigma_0 = 70$	266.56	0	67.41

6.2. A portal frame problem

In this example, the optimal topology of a portal frame structure depicted in Fig. 6 is investigated under stress constraints. As a further test of the ability of the proposed approaches to alleviate stress concentrations, three sharp re-entrant corners are set up deliberately in the design domain. We apply the problem formulation in Eq. (4.5) with $\overline{\sigma} = 1.7$ to solve the problem. The corresponding optimization results are shown in Fig. 9. Again, as expected, the stress distributions in the stress-based designs are more uniform than that of its compliance-based counterpart. Moreover, the maximum stress of 1.70 (for 120×60 mesh) in the stress-based design is significantly lower than the 2.51 in the compliance-based design. This is not surprising since the sharp re-entrant corners, which are sources of stress concentrations, has been eliminated successfully in the stress-based design. This example shows once again that the proposed global stress measure F^* does have the capability to provide a strict control of local stress in the entire region of the structure even for this challenging problem. The detailed optimization results of this problem are reported in Table.2.

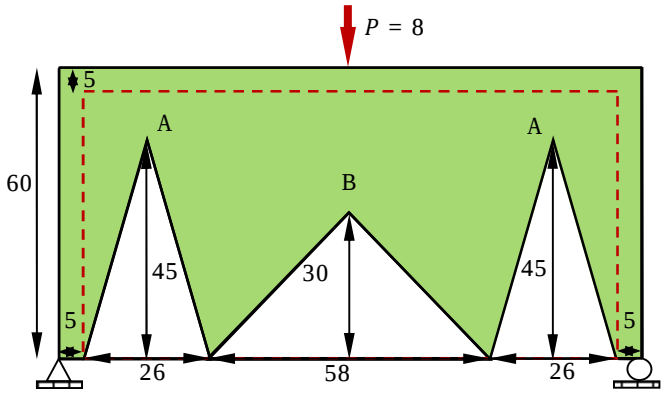

Fig. 6 Design domain of the portal frame problem.

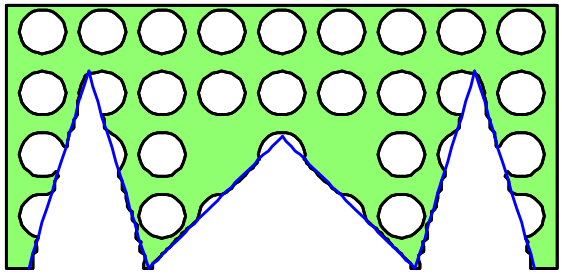

Fig. 7 Initial design of the portal frame problem.

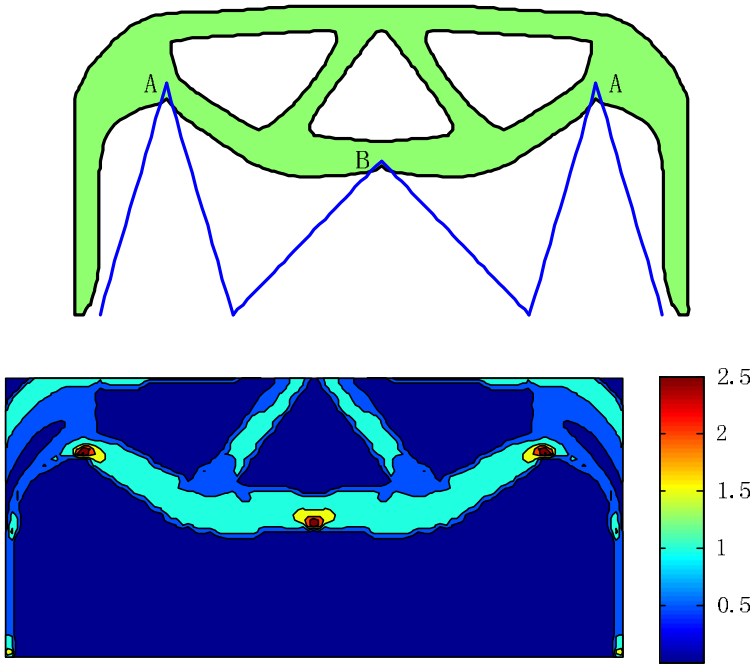

Fig. 8 Compliance-based optimal design of the portal frame problem and the corresponding stress distribution.

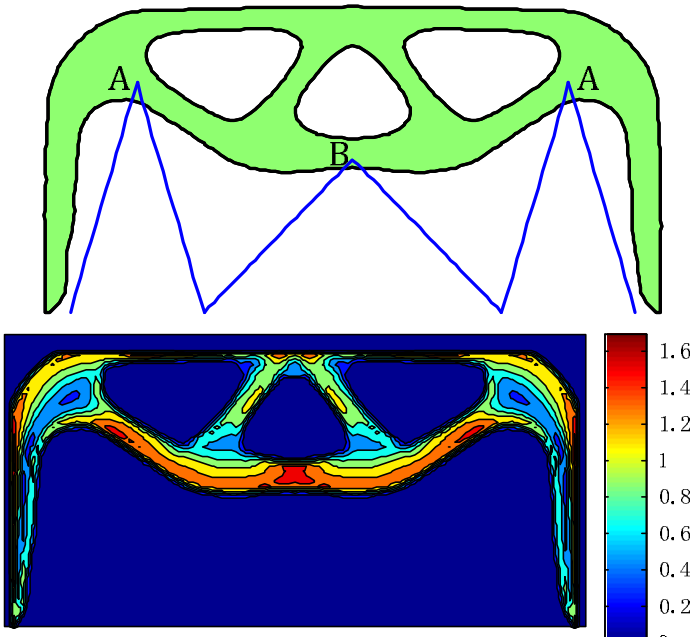

Fig. 9 Optimal design of the portal frame problem and the corresponding stress distribution with 120×60 mesh ($\bar{\sigma} = 1.7$) under formulation Eq. (4.5).

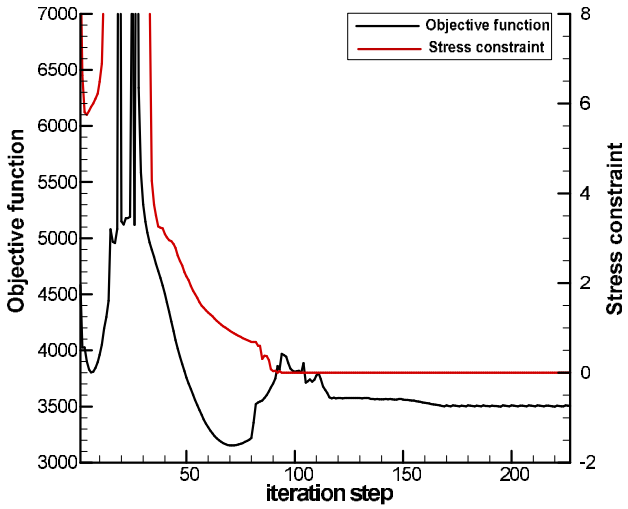

Fig. 10 Iteration history (120×60 mesh, $\bar{\sigma} = 1.7$).

Table.2 Optimization results for the portal frame problem

	Compliance	Stress constraint	von Mises stress at A/B
Compliance minimization	3405.3	/	2.5108/2.4172
60×120 with $\sigma_0 = 1.7$	3506.8	0	1.6762/1.7003

7. Conclusion

In the present paper, topology design of continuum structures with less stress concentration is discussed in level set framework using a new global stress measures. The proposed approaches allow us to deal with large-scale stress-related topology optimization problems with reasonable computational cost. Numerical examples demonstrate that local stress level can be reduced substantially via the new stress measures with reasonable computational cost. The measure F^* with stress gradient enhancement is versatile in the sense that it

can deal with general situations of stress concentration and no artificial parameters are required in numerical implementations. Our study also indicates that level set-based approach coupled with X-FEM method is a promising way for the solution of stress-constrained topology optimization problems under appropriate formulations.

5. Acknowledgements

The financial support from the National Natural Science Foundation (10932003, 10925209 and 91216201), 973 Project of China (2010CB832703), Program for Changjiang Scholars and Innovative Research Team in University (PCSIRT) and the Fundamental Research Funds for the Central Universities (DUT11ZD104) is gratefully acknowledged.

6. References

[1] M.P. Bendsoe and N. Kikuchi, Generating optimal topologies in structural design using a homogenization method, *Computer Methods in Applied Mechanics and Engineering*, 71, 197-224, 1988.

[2] H.A. Eschenauer, and N. Olhoff, Topology optimization of continuum structures: A review, *Applied Mechanics Reviews*, 54, 331-390, 2001.

[3] M.P. Bendsoe, E. Lund, N. Olhoff and O. Sigmund, Topology optimization-broadening the areas of application, *Control and Cybernetics*, 34, 7-35, 2005.

[4] X. Guo and G.D. Cheng, Recent development in structural design and optimization, *Acta Mechanica Sinica*,26, 807-823, 2010.

[5] G.I.N. Rozavany and T. Birker, On singular topologies in exact layout optimization, *Structural Optimization*, 8, 225-232, 1994.

[6] M.P. Bendsoe and O. Sigmund, Topology Optimization: Theory, Methods and Applications, Springer-Verlag, Berlin, 2003.

[7] G.D. Cheng and X. Guo, ϵ-relaxed approach in structural topology optimization, *Structural Optimization*, 13, 258–266, 1997.

[8] G. Allaire and F. Jouve, Minimum stress optimal design with the level set method, *Engineering Analysis with Boundary Elements*, 32, 909-918, 2008.

[9] X. Guo, W.S. Zhang, M.Y. Wang and Wei P. Stress-related topology optimization via level set approach, *Computer Methods in Applied Mechanics and Engineering*; 200, 3439-3452, 2011.

[10] P. Wei, M.Y. Wang, X.H. Xing, A study on X-FEM in continuum structural optimization using a level set Model, *Computer Aided Design*, 42, 708-719, 2010.